Zhang, S., Kong, D., Mellios, E., Doufexi, A., & Nix, A. (2016). Comparing theoretic single-user and multi-user full-dimension MIMO data throughputs in realistic city-wide LTE-a deployments. In 2015 IEEE Global Communications Conference (GLOBECOM 2015): Proceedings of a meeting held 6-10 December 2015, San Diego, California, USA. (pp. 3440-3446). [7417502] Institute of Electrical and Electronics Engineers (IEEE). DOI: 10.1109/GLOCOM.2014.7417502

# Comparing Theoretic Single-User and Multi-User Full-Dimension MIMO Data Throughputs in Realistic City-Wide LTE-A Deployments

Siming Zhang, Di Kong, Evangelos Mellios, Angela Doufexi and Andrew Nix

Communication Systems & Networks Group
University of Bristol, United Kingdom

{sz1659; d.kong; evangelos.mellios; A.Doufexi; andy.nix}@bristol.ac.uk

***Abstract*— This paper evaluates the theoretic performance of multi-user multiple-input-multiple-output (MU-MIMO) systems in heterogeneous LTE-Advanced urban environments (i.e. Macrocells and Picocells) using classic Eigen-Beamforming (EBF) and Block Diagonalisation (BD) precoding methods. The work quantifies the realistically achievable improvement of MU-MIMO compared with traditional single-user (SU) MIMO schemes. In addition, the impact on system level capacity of different Base Station (BS) antenna numbers and array geometries are investigated. A 3D ray-tracing channel propagation model of the City of Bristol (UK) was used along with measured 3D polarimetric antenna patterns for the individual BS and UE elements. More than one million ray-traced Pico and Macro cellular links were evaluated to ensure statistical relevance. Our analysis quantifies the capacity of an 8×8 Full-Dimension MU-MIMO solution in realistic urban heterogeneous environments addressing single-antenna and dual-antenna UEs. Results address the system level benefits of increasing the number of BS and UE antenna elements as well as the sensitivity of capacity to vertical and horizontal spatial element configurations at the BS.**

***Keywords— LTE-A; 3D Ray-Tracing Channel Model; FD-MIMO; SU-MIMO vs. MU-MIMO; Single/Dual-antenna UEs.***

## I. INTRODUCTION

Long Term Evolution (LTE) Release-8 [1] is being commercialized all around the globe for 4G cellular broadband wireless connectivity. Its air interface provides single-user multiple-input-multiple-output (SU-MIMO) with up to 4 transmit antennas in the downlink (DL). In Releases 10 [2], also known as LTE-Advanced (LTE-A), SU-MIMO technologies are extended to support 8 antennas at the base station (BS), meanwhile multi-user (MU) MIMO has been recognised as a critical technique to further enhance spectral efficiency. Release 11/12 further adds Full-Dimension (FD) Beamforming, coordinated multipoint (CoMP) transmission and reception and support for heterogeneous deployment [3].

Many papers, for example [4]-[6], have addressed SU-MIMO performance through simulation or measurement in LTE-A networks; in particular they address how much capacity improvement can be achieved using excess antenna elements at the base station. Our previous work [7] has demonstrated impressive capacity gain in both average cell throughput and cell-edge user throughputs in a 16Tx–8Rx system compared to an 8Tx–8Rx system in heterogeneous LTE-A deployments. We have also observed in realistic channels that the number of useable spatial streams is far less than the maximum number of antenna ports at the UE, highlighting the importance of performing real-world evaluations. In this paper we analyze the performance of 8×8 and 16×8 systems with MU-MIMO transmissions to single-antenna or dual-antenna users.

As for MU-MIMO, [8] quantifies the throughput improvements with MU-MIMO over SU-MIMO as a function of the propagation environment, antenna configuration and interference suppression capability of the single-antenna users in a 4Tx – 2Rx system. One interesting observation was the MU-MIMO performance of closely spaced uniform linear array is significantly better than that of cross-polarized antenna arrays. [9] investigated the performance of Full-Dimension MIMO in LTE-A and beyond cellular networks with various 2D antenna array configurations. It was observed that FD-MIMO system could improve the cell average throughput and the 5-percentile user throughputs by a factor of 5 when using 64 instead of 8 elements at the BS using standard channel models. Results in [10] showed that horizontal elements are more favourable than vertical elements and larger antenna element spacings are desired in both 3D Urban Macro (UMa) and Urban Micro (UMi) scenarios.

The main contributions of this paper are listed below:

- All the quantitative conclusions are based on a realistic 3D ray-traced channel model (ProPhecy) [11] performed at city scale for urban Picocells and Macrocells. This model was used to generate many of the statistics now specified in the 3D extension of the 3GPP (The 3rd Generation Partnership Project) channel model [12-14]. ProPhecy makes use of a 3D laser-scanned environmental database (in this work a database for the city of Bristol (UK) was used). Antenna characteristics are omitted from the 3GPP channel model yet play a significant role in determining MIMO capacity. 3D complex voltage and polarimetric antenna patterns for the individual BS and UE antenna elements were measured in our anechoic chamber. Meanwhile, realistic linear array and 2-D planar array geometries are deployed to harvest the channel capacity in azimuth and elevation domains, hence FD-MIMO.

- We have extended the evaluation of the MU-MIMO LTE-A system configuration from traditional 4Tx – 2Rx (Release 8) and 8Tx – 4Rx (Release 10) to the higher-order 8Tx – 8Rx and 16Tx – 8Rx. We have investigated two classic channel precoding methods, i.e. Eigen-Beamforming (EBF) and Block Diagonalisation (BD). Also, link adaptation is performed on a per UE basis in order to optimise the expected cell capacity.
- We quantify capacity improvement as a function of the number of BS antenna elements and their array geometries, the propagation environment and the use of single- or dual-antennas at the UE. [7] discusses the methodology adopted in this paper (although here we have extended the approach to support MU-MIMO). Given our previous SU performance results, direct comparisons are made in SU- and MU-MIMO systems.
- The number of link-level simulations in this study accumulates to 1,108,000 to ensure our results are statistically relevant. To the best of the authors' knowledge, no other work has been reported at this scale.

The remainder of the paper is organised as follows: Section II presents the measured BS and UE antenna element characteristics and array configurations. Section III explains our 3D channel propagation modelling process. Section IV introduces our LTE-A DL network simulator with EBF and BD precoding methods, as well as the associated RBIR (the Received Bit level mutual Information Rate) abstraction technique [15]. Simulation results in the form of expected user throughput, statistics for the number of supported spatial streams and outage probabilities are given in Section V. Finally, Section VI summarises the comparison of large-scale 3D SU and MU MIMO for heterogeneous LTE-A deployment.

## II. ANTENNA CHARACTERISITCS AND CONFIGURATIONS

### A. Measured BS and UE Antenna Element Statistics

As can be seen in Fig. 1(a) (left column), each Macro BS antenna element is a measured directional patch antenna on RT/Duroid 5880 substrate. The far-field antenna patterns of two orthogonally polarised patch antennas are shown in Fig. 1(a) (right column). V and H refer to the vertical and horizontal polarisation components of the radiation pattern respectively with orange and blue colouring. The azimuth and elevation 3dB beamwidths of the Macro BS (total power) patterns are 88° and 72° respectively for *Ant 1*, and 91° and 71° for *Ant* 2. Fig. 1(b) shows the Pico cell BS/UE antenna element, which comprises of a vertical (z-directed) and a horizontal (y-directed) dipole. Table I lists the percentages of radiated power in both vertical and horizontal polarisations for both antenna elements at the Macro and Pico BS, along with the maximum directivity for each polarisation.

The BS array was down-tilted by 10° in our virtual network simulations to optimise the in-cell signal to noise ratio (SNR). Variations of the shadowing across the base station or mobile antenna arrays are not modelled in this work, since the dimensions of the antenna arrays are relatively small at 2.6GHz operating frequency and the effect of shadowing is negligible.

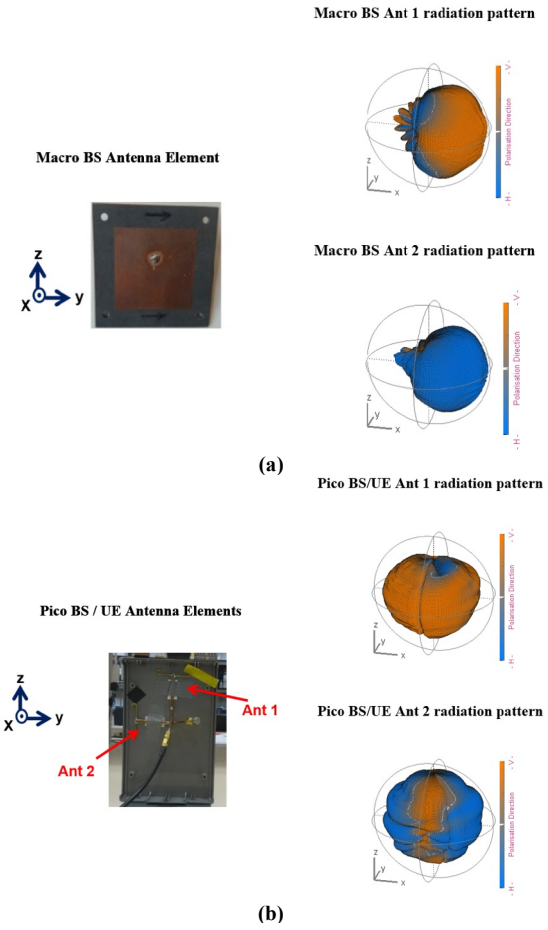


Fig. 1. Antenna elements and radiation patterns for Macro/ Pico BS and UE

TABLE I. BS AND UE ANTENNA POWER STATISTICS

| | Percentage Power in each polarisation | | Max. directivity in each polarisation (dBi) | |
|---|---|---|---|---|
| | *Vertical* | *Horizontal* | *Vertical* | *Horizontal* |
| **Macro BS Ant 1** | 83% | 17% | 8.00 | -0.49 |
| **Macro BS Ant 2** | 5% | 95% | -5.96 | 8.02 |
| **Pico BS/UE Ant 1** | 90% | 10% | 5.42 | -3.77 |
| **Pico BS/UE Ant 2** | 33% | 67% | 3.93 | 5.35 |

### B. BS and UE Antenna Configurations

Fig. 2(a) shows the four different BS (Macro and Pico) antenna configurations investigated in this paper. The color of the wording in Fig. 2(a) corresponds to the antenna spatial placements illustrated below. The 'X' corresponds to two co-located cross-polarised logical antennas. The UE antenna number and the 2D spatial arrangements (Fig. 2(b)) were fixed for the SU-MIMO simulations at 8 mixed elements, while in MU-MIMO cases, single-antenna and dual-antenna UEs were considered, i.e. 8 single-antenna UEs or 4 dual-antenna UEs. In all cases half-wavelength antenna spacing was assumed.

## III. CHANNEL MODEL AND RAY-TRACING

The channel propagation study was performed using the University of Bristol's outdoor 3D ray-tracer [11]. A 17.6km2 laser-scanned database of the City of Bristol (UK) was used. The database comprises buildings, foliage and terrain layers at 10m resolution. Table II shows a summary of the ray-tracing parameters used in this study. A detailed statistical analysis of the propagation parameters can be found in [16, 17]. Note that antennas were assumed isotropic at both ends of the link in the propagation model allowing us to generate a pure channel. In post processing any type of transmit and receive antenna pattern and geometry can then be applied as a spatial-polarisation-phase convolution process.

Point-source ray-tracing was performed from the BS to each UE location following the procedure described in [18]. Fig. 3 illustrates the traced multipath rays in a MU-MIMO scenario for a Picocell and a sectorised Macrocell. The underlying colour of the rays indicates the received power, the brighter the colour the higher the power. The ray model provides information not only on the amplitude, but phase, time delay, angle-of-departure (AoD) and angle-of-arrival (AoA) of each multipath component (MPC) linking the BS and UE. The phase of each MPC was then adjusted according to the transmitting/receiving antenna's relative distance from a zero-phase reference point on the array. The complex gain of each MPC was also adjusted according to the transmitting/receiving antenna E-field pattern response for the corresponding AoD/AoA and polarization.

## IV. NETWORK SIMULATOR AND PARAMETERS

In order to quantify data throughput performance, a LTE-A downlink simulator was implemented in MATLAB. Table III lists the key parameters of this simulator. The full Channel State Information (CSI) was assumed to be available at the BS. Therefore, two closed-loop channel precoding methods, Eigen-Beamforming (EBF) and Block Diagonalisation (BD), were evaluated and compared.

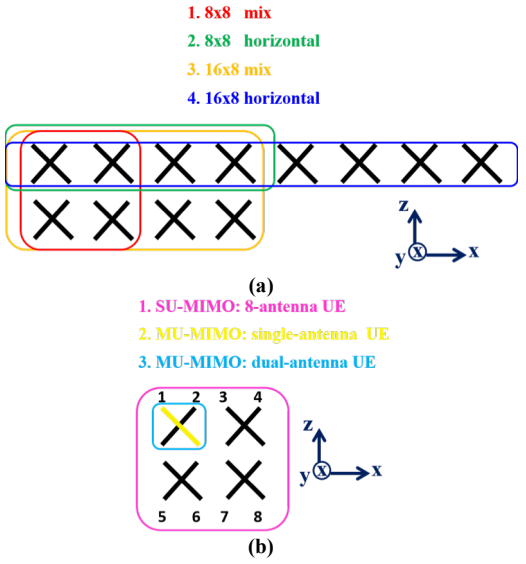


Fig. 2. Antenna spatial geometries at (a) Macro/Pico BS, (b) UE *(the inter-element spacing is assumed to be equal both horizontally and vertically)*

TABLE II. SUMMARY OF RAY-TRACING PARAMETERS

| | **Macro cells** | **Pico cells** |
|---|---|---|
| **Environment** | 17.6km$^2$ area of central Bristol (UK) | |
| **Frequency** | 2.6 GHz | |
| **BS mounting** | On rooftops of buildings at a height of 3m above rooftop level | On lamp-posts at a height of 5m above ground level |
| **Number of BSs and UEs** | 20 three-sector cells 300 random UEs per sector (Total 900 UEs) | 20 cells 150 random UEs per cell |
| **User locations** | 50-1000 m from BS 1.5m above ground level | 5-150 m from BS 1.5m above ground level |
| **BS transmit power** | 44 dBm | 30 dBm |
| **BS height** | Ranging from 7m to 50m | 5 m above ground level |
| **Antennas** | Isotropic at both ends of the link | |
| **Minimum receiver sensitivity** | -120 dBm (only links with two or more traced rays were considered) | |
| **Link direction** | Downlink (From BS to UE) | |

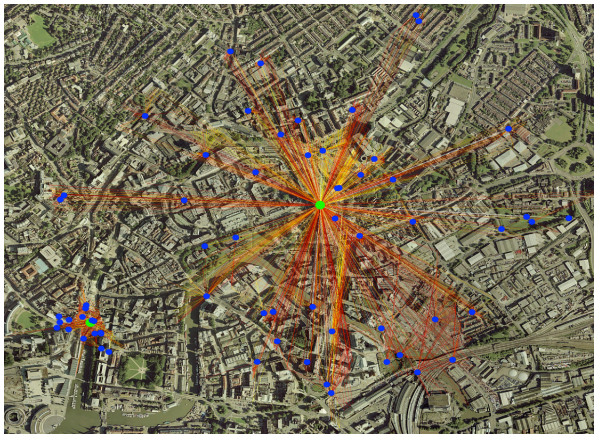

Fig. 3. Modelling of MPCs for 3-D MU-MIMO in a sectorised Macrocell and Picocell (*green dots: BS locations, blue dots: UE locations*)

The following notations will be used across this paper. Normal letters represent scalar quantities and bold uppercase letters denotes matrices. $|.|$, $(.)^T$, and $(.)^H$ are determinant, transpose, and Hermitian operators respectively.

### A. Eigen-Beamforming

Traditional eigenvalue-based MU beamforming obtains the precoding weights $\boldsymbol{W}_k$ for user $k$ in a system comprising of $K$ total users from the singular value decomposition (SVD) of the UE's frequency domain channel matrix $\boldsymbol{H}_k$:

$$\boldsymbol{H}_k = \boldsymbol{U}_k \boldsymbol{S}_k \boldsymbol{V}_k{}^H \qquad (1)$$

$\boldsymbol{W}_k$ is the eigenvectors in $\boldsymbol{V}_k$ corresponding to the $n_{r,k}$ (the number of receive antennas of user $k$, here we assume the user has the same number of RF chains) largest eigenvalues of matrix $\boldsymbol{H}_k^H \boldsymbol{H}_k$. The theoretic capacity of user $k$ can be calculated as:

$$C_k = log_2 \left| \boldsymbol{I} + \frac{\boldsymbol{H}_k \boldsymbol{W}_k \boldsymbol{W}_k^H \boldsymbol{H}_k^H}{(\delta_n^2 \boldsymbol{I} + \sum_{i=1, i \neq k}^{K} \boldsymbol{H}_k \boldsymbol{W}_i \boldsymbol{W}_i^H \boldsymbol{H}_k^H)} \right| \qquad (2)$$

TABLE III. SUMMARY OF SIMULATION PARAMETERS

| Parameter | Assumption |
|---|---|
| **Transmission bandwidth** | 20 MHz |
| **FFT size** | 2048 |
| **Number of occupied subcarrier** | 1200 |
| **Number of OFDM symbols per time slot** | 7 |
| **Channel State Information** | Perfect |
| **Channel coding** | Turbo |
| **Noise floor** | -96 dBm |
| **PER threshold** | 0.1 |
| **MCS modes** | QPSK1/2,QPSK3/4,16QAM1/2, 16QAM3/4,64QAM1/2,64QAM3/4 |
| **MIMO precoding** | 8x8/16x8 SU-EBF, MU-EBF and MU-BD |
| **UE Configuration (SU/MU)** | 8-antenna UE/ Single-antenna or Dual-antenna UE |
| **SNR range for MU-MIMO** | -20 dB to 25 dB |
| **Multi-User Grouping** | 100 random iteration per sector/cell |
| **Peak Capacity** | 604.8 Mbps |

where $\delta_n^2 I$ denotes the Additive White Gaussian Noise and the summation part of the formula represents the interference from all the other $(K-1)$ users in the system. This precoding method aims to maximise the signal power for each user but fails to mitigate the multiuser interference, resulting in an interference-limited system at high SNRs [19]. It is important to note that our approach is based on the EBF concept but jointly considering the overall channel matrix comprising all users. Through investigating the eigen-structure of the channel, along with the help of a physical (PHY) layer abstraction engine (known as RBIR and discussed in Section C) we can accurately and efficiently estimate the system-level capacity. Note that this approach does increase the computation requirement, and scales with system configuration.

### B. Block Diagonalisation

The Block Diagonalisation algorithm is a classic linear zero-forcing algorithm for MU-MIMO with multi-antenna UEs [20]. It works in situations when the number of transmit antennas is no less than the total number of receive antennas. It eliminates the multiuser interference completely by forcing the precoding matrix of one user to lie in the null space of other users' channel matrices, which is called the constraint matrix for user $k$:

$$\widehat{\boldsymbol{H}_k} = [\boldsymbol{H}_1^T \dots \boldsymbol{H}_{k-1}^T \quad \boldsymbol{H}_{k+1}^T \dots \boldsymbol{H}_K^T]^T \qquad (3)$$

SVD is performed to find the null space of the constraint matrix:

$$\widehat{\boldsymbol{H}_k} = \widehat{\boldsymbol{U}_k}\widehat{\boldsymbol{S}_k}\left[\widehat{\boldsymbol{V}_k}^{(1)} \ \widehat{\boldsymbol{V}_k}^{(0)}\right]^H \qquad (4)$$

Hence, $\boldsymbol{H}_k\widehat{\boldsymbol{V}_k}^{(0)}$ represents the projection of $\boldsymbol{H}_k$ in the null space of $\widehat{\boldsymbol{H}_k}$. The non-zero eigenvectors in this projection can be obtained once again through SVD:

$$\boldsymbol{H}_k\widehat{\boldsymbol{V}_k}^{(0)} = \boldsymbol{U}_k\boldsymbol{S}_k[\boldsymbol{V}_k^{(1)} \ \boldsymbol{V}_k^{(0)}]^H \qquad (5)$$

Thereafter, the precoding matrix of user $k$ is simply given as:

$$\boldsymbol{W}_k = \widehat{\boldsymbol{V}_k}^{(0)}\boldsymbol{V}_k^{(1)} \qquad (6)$$

BD effectively transforms MU-MIMO channel into multiple parallel SU-MIMO channels, ready to be used with RBIR. This approach is mainly noise-limited and performs poorly at low SNR [19]. In addition, [20] shows when users have highly correlated channels at high SNRs, capacity degrades significantly due to limited orthogonal space between users.

### C. Abstraction Simulator

To perform system level analysis in a computationally efficient and scalable manner, a PHY layer abstraction technique RBIR was used to predict the packet error rate (PER) for a given channel realisation across the allocated OFDM subcarriers. This technique was fully described in [15] and subsequently used in a number of our Wireless LAN and cellular network studies, for instance [21] and [22]. Without sacrificing accuracy, abstraction is many hundreds of times faster than full bit-level simulation.

Optimal modulation and coding scheme (MCS) selection was performed per UE based on the mode that achieved the highest link throughput on the condition that the PER does not exceed 10%. The expected throughput was then calculated using the peak error-free data rate (for the supported number of spatial streams and MCS) and the PER, and averaged over 1000 channel realisations. Although theoretic SNR values can be very high, in practice Error Vector Magnitude (EVM) specifications limit the maximum SNR observed at the UE. For this study we assumed a peak SNR of 25dB at the UE (which translates to an EVM of around 6%). Furthermore, any UE locations with an SNR below -20 dB were excluded from MU-MIMO analysis. Finally, the transmit power for each UE is equally allocated in the system, while maintaining a normalised total power constraint of unity.

## V. RESULTS AND DISCUSSIONS

Fig.4 shows the Cumulative Distribution Function (CDF) plots of the optimum achievable data throughputs in both Macro and Pico cell scenarios for SU- and MU-MIMO. Note that the BS array is horizontally configured and users in the MU cases are equipped with dual antennas. It can be seen that the Picocells outperform the Macrocells in terms of data throughput. This occurs because of the higher received signal powers and the greater angular spreads in both the azimuth and elevation domains in Picocells. For the standard 8×8 configuration MU-EBF offers the best capacity compared to the SU-EBF and MU-BD schemes. Additionally, SU-EBF has more than twice the average data rate than MU-BD in Macrocells, while the two schemes are very closely matched in the Picocells, yielding a mean throughout of around 150Mbps, notwithstanding the peak data rate of just over 600Mbps. This interesting observation confirms the inherent disadvantage of the BD algorithm in low SNR scenarios in Macrocells; Picocells however provide greater de-correlation between user channels to allow more streams to be supported in MU-BD.

It is expected that by increasing the BS antenna number from 8 to 16, significant capacity gain should be observed.

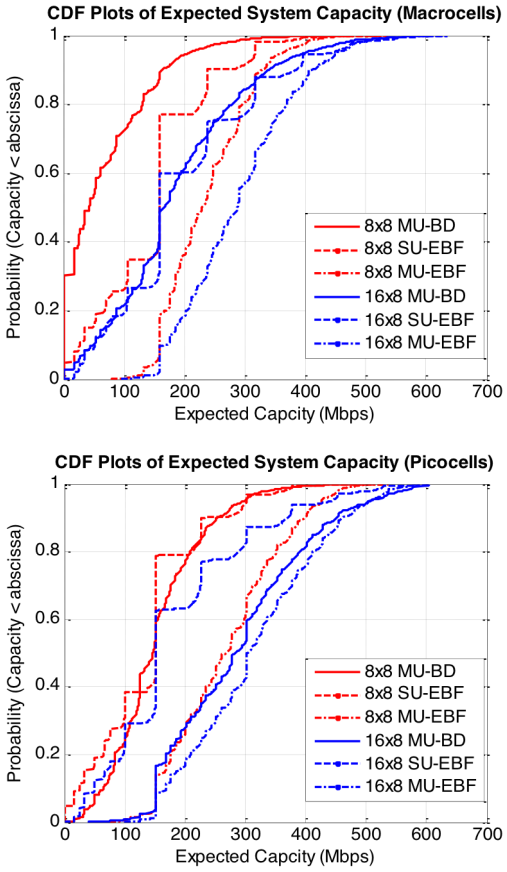


Fig. 4. CDF plots of average capacity in various system configurations

TABLE IV. 5 PERCENTILE THROUGHPUT IN VARIOUS CONFIGURATIONS

| 5%-tile throughput (Mbps) | MU-BD 8x8 | SU-EBF 8x8 | MU-EBF 8x8 | MU-BD 16x8 | SU-EBF 16x8 | MU-EBF 16x8 |
|---|---|---|---|---|---|---|
| **Macrocells** | 0 | 15.64 | 147.0 | 23.17 | 31.48 | 151.2 |
| **Picocells** | 47.69 | 15.74 | 151.2 | 151.2 | 32.84 | 151.2 |

However, 8×8 MU-EBF scheme seems to outperform 16×8 SU-EBF and 16×8 MU-BD schemes in Macrocells. This shows the advantage of MU-MIMO over SU-MIMO. At the same time, it emphases the importance of an efficient MU precoding method. In Picocells, the benefit of using 16 antennas and MU-MIMO is more visible. With the best system configuration, i.e. 16×8 MU-EBF, the expected median data rate is around half of the error-free peak rate in both Picocells and Macrocells, which is very encouraging considering the percentages is only a quarter in 16x8 SU-EBF Macrocells and Picocells. Comparing with our previous SU study, 16x8 achieved one third and one sixth of the system peak rate in Pico and Macro cells respectively [7]. The differences in SU performance can be explained by the antenna elements used. Previously, Macro BS element was a measured 10 vertically stacked patch antenna array panel with around 18dBi gain both vertically and horizontally, which is much higher than the 8dBi value assumed in this study; Pico BS element however had 3 dB less in gain. This stresses the importance of antenna characteristics in assessing cell capacity.

Table IV lists the 5 percentile rates for the various scenarios under consideration. The previous claims of average cell capacity stand true for cell-edge user throughputs. Note that MU-EBF 8 × 8 and 16 × 8 schemes demonstrate extremely good performance. Rates in excess of 150Mbps are seen for the lower 5% of users in both the Macrocells and Picocells. This represents a significant Quality of Service (QoS) enhancement compared to the SU-MIMO cases with 9-fold and 4-fold increases for 8×8 and 16×8 respectively in Macrocells. However, it is worth noting that an exhaustive search of all MCS modes and supported numbers of spatial streams was performed for all users in this study. This enables rapid switching to and from higher spatial stream numbers on a channel snapshot-by- snapshot basis. In a practical system, such gains in data rate will be less outstanding since the link speed selection algorithm is unlikely to switch so rapidly.

Fig. 5 shows the spectral efficiency performances for the MU-MIMO cases with single- and dual-antenna UEs. Note that the results are for horizontally configured BS array. This time the conclusion is straightforward: dual-antenna UEs outperform single-antenna UEs in every scenario without exception. Same conclusion was drawn in [8]. For MU-MIMO either rank 1 or rank 2 can be used for each user (i.e., one or two data streams per user). In EBF, rank 2 can provide capacity gains, while in BD it could help with interference mitigation. In Picocells there is a clear benefit when using EBF precoding and more antenna elements at the BS. However, in Macrocells, 16x8-BD performance was less satisfactory for two suspected reasons: 1) eigen-structure of the whole channel matrix may not support that many users lying in each other's null space; and 2) limitations in the UE grouping method. The random UE

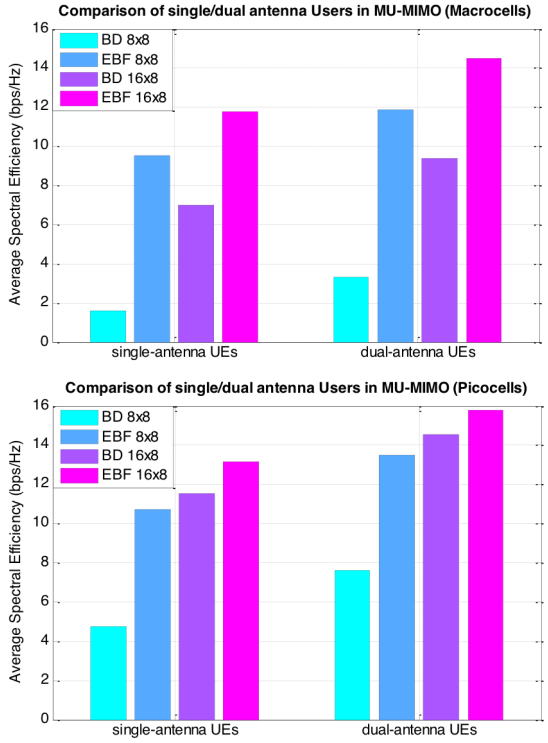


Fig. 5. Spectral efficiency comparison of single and dual antenna UEs in MU-MIMO in Macrocells and Picocells

scheduling provides only basic fairness across the network, but this introduces the problem of having drastically different SNR values by being physically near or very far from the cell centre. Since the transmit power was shared equally between data streams/UEs, cell-edge users are still not able to connect while mid-cell users suffer low SNRs.

Fig.6 focuses on the comparison between the two BS antenna array geometries used in our simulations for both SU- and MU-MIMO, i.e. mixed and horizontal. Note in MU-MIMO the users make use of dual-antennas. In Macrocells the horizontal configuration consistently offers better spectral efficiency than the mixed configuration. Similar observations were presented in [10]. Such a phenomenon is partially due to the fact that UEs are all on the similar elevation level (1.5m above ground level) and the beams in elevation are not narrow enough to enable separation. As the number of antenna elements are reduced in the horizontal axis and increased in the vertical axis, FD-MIMO loses its ability of generating narrow beams in the azimuth plane but fails to gain much additional multiplexing capability in the elevation direction. In Picocells however the mixed configuration exceeds the horizontal configuration in the SU 8×8 and SU 16x8 cases by 22% and 26% respectively. This trend agrees with our previous work and the reason goes back to the greater angular spreads in both the azimuth and elevation domains in Picocells. In addition, in SU-MIMO receiver antennas are closely packed and does not need sharp spatial beams but rely on the channel richness to support more data streams, hence the benefit of exploring the elevation domain of the channels. Vertical BS antenna elements better explore that angular statistics. Furthermore, when relating back to the dipoles used at Pico BS, they have characteristically wider 3dB beamwidths than patches in their far-field radiation patterns enabling them to capture more rays coming from wider angles.

Fig.7 illustrates the histograms of driving 1 to 8 spatial data streams between the BS and the UEs in Macrocells and Picocells for 8×8 and 16×8. Here only the horizontal BS array configuration and MU-MIMO with dual-antenna UEs are shown. Table V is an empirical summary of the average supported streams from Fig.7. Overall, the expected number of spatial data streams is 4 or 5 for Picocells and Macrocells with 8×8 MU-EBF. While with the MU-BD scheme, only 1 or 2 spatial streams are achieved in Macrocells and 3 or 4 in Picocells on average. When 16 antennas are deployed at the BS, one extra stream is achieved on average. This occurs because the additional degrees of freedom provide a diversity gain that lowers the SNR required to drive a given spatial stream number. It is also worth mentioning that more than 10% of the links are able to support higher spatial streams (i.e. 7 or 8 streams) for MU 16×8 in Picocells. Furthermore, the ability to have full rank (and hence realise the peak data rates available in LTE-A) is only feasible using the MU 16×8 configuration using either precoding methods in both Macro and Picocells.

Table VI presents the outage improvements going from 8×8 to 16×8, SU to MU. Here, outage means either a connection cannot be established between the BS and UE, or the link does not comply with the constraint of a PER less than 10%. In Macrocells, a significant outage probability of about 30% was observed for SU (8×8 and 16×8) and MU-BD (8×8). As for SU

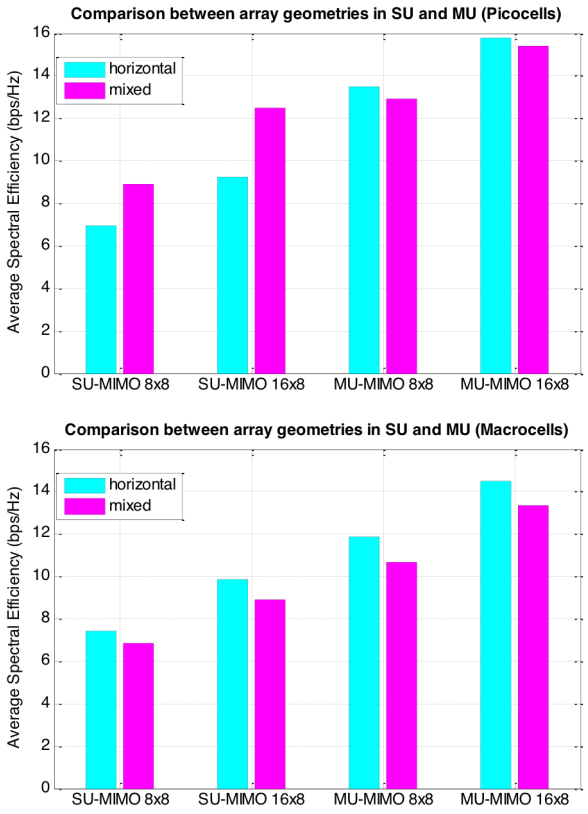


Fig. 6. Spectral efficiency comparison between mix and horizontal BS gemotries in SU and MU-MIMO in Macrocells and Picocells

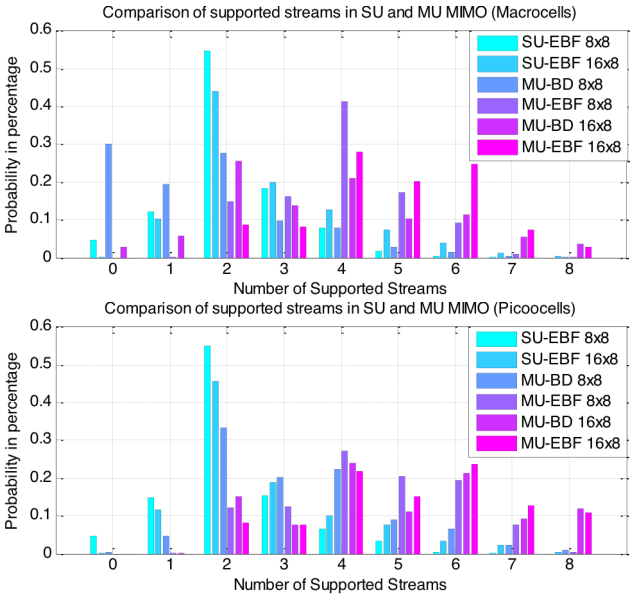


Fig. 7. Probabilities of supporting *1 to 8 data* streams in various scenarios

TABLE V. AVERAGE SUPPORTED DATA STREAMS

| Supported Number of Streams | SU-EBF 8x8 | SU-EBF 16x8 | MU-BD 8x8 | MU-EBF 8x8 | MU-BD 16x8 | MU-EBF 16x8 |
|---|---|---|---|---|---|---|
| **Macrocells** | 2.19 | 2.81 | 1.64 | 3.93 | 3.71 | 4.78 |

| | | | | | | |
|---|---|---|---|---|---|---|
| **Picocells** | 2.16 | 2.77 | 3.30 | 4.46 | 4.91 | 5.19 |

TABLE VI. PROBABILITIES OF NO STREAMS SUPPORTED

| Outage Probability (%) | SU-EBF 8x8 | SU-EBF 16x8 | MU-BD 8x8 Single /Dual | MU-EBF 8x8 Single /Dual | MU-BD 16x8 Single /Dual | MU-EBF 16x8 Single/ Dual |
|---|---|---|---|---|---|---|
| **Macrocells** | 30.4 | 27.7 | 41.3/ 28.6 | 0/ 0 | 2.0/ 2.7 | 0/ 0 |
| **Picocells** | 4.3 | 0.17 | 0.4/ 0.2 | 0/ 0 | 0/ 0 | 0/ 0 |

case, this number is higher than that quoted in our previous work mainly due to the antenna element gain difference. The outage probabilities are much better in Picocells in the same scenarios. Astonishingly, MU-EBF is able to eliminate outage completely in both the 8×8 and 16×8 configurations (Macrocells and Picocells). Here it means in actuality there is always at least one UE being serviced with MU-MIMO. Although reduced outage is very important to perceived network performance (this greatly enhances the experience of users with low SNR, e.g. cell edge users), and contributes to the gain in expected throughput, its impact is small since the mean value is dominated by the higher rate links.

## VI. CONCLUSIONS

This work has quantified the system level benefits of upgrading SU-MIMO to MU-MIMO in terms of average cell capacity and spectral efficiency, 5 percentile user throughputs, the number of supported data streams and the outage probability in urban LTE-A deployments. Investigations were performed in city scale realistic environments using accurate propagation models, measured antenna patterns and practical array geometries. This work has highlighted the importance of performing real-world evaluations, since many simpler channel models significantly over-predict the potential capacity of an LTE-A system.

Overall, in realistic channels, MU-MIMO (16×8 with dual-antenna UEs) provided up to 95% and 128% capacity improvement over SU-MIMO (16×8) in Macrocells and Picocells. MU supported more than 5 spatial streams on average with 4 dual-antenna UEs, compared with less than 3 streams in the 8-antenna SU case. EBF precoding scheme consistently outperformed BD in terms of overall cell capacity. Dual-antenna UEs achieved approximately 20-30% more capacity than single-antennas UEs in both Macrocells and Picocells. In most cases we found that a BS with horizontally placed antennas achieved higher capacity. In terms of Quality of Service an impressive reduction in the outage probability of cell-edge users was observed with MU-MIMO.

## ACKNOWLEDGMENTS

The authors would like to acknowledge the technical and financial support of Timothy Thomas and Amitava Ghosh at Nokia Networks (Chicago, USA).

## REFERENCES

[1] 3GPP TS 36.201: "*Evolved Universal Terrestrial Radio Access (E-UTRA); Physical Channels and Modulation (Release 8)*", 2009.

[2] "*3GPP Release 10 V0.1.1, Overview of 3GPP*," 2011.

[3] Ericsson white paper, "*LTE RELEASE 12*," 2013, (*http://www.ericsson.com/res/docs/whitepapers/wp-lte-release-12.pdf)*.

[4] J. Lee, J.-K. Han, and J. Zhang, "*MIMO technologies in 3GPP LTE and LTE-advanced*," Eurasip Journal on Wireless Communications and Networking, vol. 2009, no. 1, Article ID 302092, 2009.

[5] Z. Mansor, E. Mellios, A. Nix, J. McGeehan, and G. Hilton, "*Impact of antenna patterns and orientations in heterogeneous LTE-Advanced networks*," in Proceedings of the 6th European Conference on Antennas and Propagation (EUCAP '12), pp. 1904–1908, 2012.

[6] K. Werner, H. Asplund, B. Halvarsson, N. Jalden, and D.V.P. Figueiredo, A.K. Kathrein, "*LTE-A Field Measurements: 8x8 MIMO and Carrier Aggregation*", in Proc. VTC Spring, 2013, pp.1-5.

[7] S.Zhang, D. Kong, E. Mellios, G. Hilton, A. Nix, T. Thomas, A. Ghosh, "*Impact of BS Antenna Number and Array Geometry on Single-User LTE-A Data Throughputs in Realistic Macro and Pico Cellular Environments*", IEEE Wireless Communications and Networking Conference (WCNC), 2015

[8] B. Mondal, T. Thomas, A. Ghosh, "*MU-MIMO System Performance Analysis In LTE Evolution*", IEEE 21st International Symposium on Personal Indoor and Mobile Radio Communications, 2010

[9] Y. Kim, H. Ji, H. Lee, B. Ng, J. Zhang, "*Evolution Beyond LTE-Advancedwith Full Dimension MIMO*", IEEE International Conference on Communications 2013: IEEE ICC'13 - Workshop Beyond LTE-A

[10] H. Ji, Y. Kim, Y. Kwak, J. Lee, "*Effect of 3-Dimensional Beamforming on Full Dimension MIMO in LTE-Advanced*", Globecom 2014 Workshop - Emerging Technologies for 5G Wireless Cellular Networks.

[11] K.H. Ng, E.K. Tameh, A. Doufexi, M. Hunukumbure, and A.R. Nix, "*Efficient Multi-element Ray Tracing With Site-Specific Comparisons Using Measured MIMO Channel Data*", IEEE Transactions on Vehicular Technology, vol. 56, issue 3, pp. 1019-1032, May 2007.

[12] T. Thomas, F. W. Vook, E. Visotsky et al., "*3D extension of the 3GPP/ITU channel model*," in Proceedings of the 77th IEEEVehicular TechnologiesConference (VTC-Spring), Dresden, Germany, May 2013.

[13] Text Proposal R1-130497, "*3D ChannelModeling Issues and 3D Channel Model Proposal, 3GPP TSG-RANWG1*".

[14] Text Proposal R1-130500, "*Detailed 3D Channel Model, 3GPP TSG-RANWG1*".

[15] D. Halls, A. Nix, and M. Beach, "*System level evaluation of UL and DL interference in OFDMA mobile broadband networks*," in Proceedings of the IEEE Wireless Communications and Networking Conference (WCNC '11), pp. 1271–1276,March 2011.

[16] E.Mellios, A. R.Nix, and G. S.Hilton, "*Ray-tracing urban picocell 3D propagation statistics for LTE heterogeneous networks*," in Proceedings of the 7th European Conference on Antennas and Propagation (EuCAP '13), April 2013.

[17] E. Mellios, A. R. Nix, and G. S. Hilton, "*Ray-tracing urban macrocell propagation statistics and comparison with WINNER II/+ measurements and models*," in Proceedings of the Loughborough Antennas & Propagation Conference (LAPC '12), pp. 1–4, 2012.

[18] Y.Q Bian, A.R. Nix, E.K Tameh and J.P McGeehan, 'MIMO–OFDM WLAN Architectures, Area Coverage, and Link Adaptation for Urban Hotspots,' *IEEE Trans. Veh. Tech*, vol.57, no.4, July 2008.

[19] H. Liu, X. Cheng, Z. Zhou, G. Wu, "*Block Diagonalization Eigenvalue Based Beamforming precoding design for Downlink Capacity Improvement in Multiuser MIMO channel*", International Conference on Wireless Communications and Signal Processing (WCSP), 2010

[20] M. Khan, M. Lee, "*Performance of Block Diagonalization Scheme for Multiuser MIMO Downlink Heterogeneous Channels*", 13th International Symposium on Communications and Information Technologies (ISCIT), 2013

[21] D. Kong, E. Mellios, D. Halls, A. Nix, and G. Hilton, "*Throughput sensitivity to antenna pattern and orientation in 802.11n networks*," IEEE 22nd International Symposium on Personal, Indoor and Mobile Radio Communications, pp. 809–813, 2011.

[22] D. Kong, E. Mellios, D. Halls, A. Nix, and G. Hilton, "*Closedloop antenna selection for wireless LANs with directional & omni-directional*

*elements*," in Proceedings of the IEEE 74th Vehicular Technology Conference (VTC Fall '11), pp. 1–5, September 2011.